Fragmentation dynamics of liquid-metal droplets under ultra-short laser pulses

M. M. Basko,[1,2] M. S. Krivokorytov,[2,3] A. Yu. Vinokhodov,[2,3] Yu. V. Sidelnikov,[2,4] V. M. Krivtsun,[2,4] V. V. Medvedev,[2,4] D. A. Kim,[1,2] V. O. Kompanets,[4] A. A. Lash,[2,3] and K. N. Koshelev[3,4]

[1)] *Keldysh Institute of Applied Mathematics, Moscow, Russia*

[2)] *RnD-ISAN/EUV Labs, Moscow-Troitsk, Russia*

[3)] *EUV Labs, Troitsk, Moscow, Russia*

[4)] *Institute for Spectroscopy RAS, Moscow-Troitsk, Russia*

(Dated: 22 January 2017)

We present the measurements and theoretical analysis of the deformation and fragmentation of spherical liquid-metal drops by picosecond and subpicosecond laser pulses. In the experiments, 60-μm droplets of Sn-In alloy were irradiated by Ti:Sa laser pulses with a peak energy fluence of ~ 100 J/cm^2. The observed evolution of the droplet shape dramatically differs from that previously reported for nanosecond pulses. Invoking 2D hydrodynamic simulations, we explain how, due to the specifics of matter dynamics in the liquid-vapor phase coexistence region, a liquid droplet is transformed into a characteristic acorn-like expanding shell with two inner cavities. High sensitivity of the measured shell parameters to the details of the equation of state and metastable dynamics suggests that such experiments offer new possibilities in exploration of thermophysical properties of metals in the region of liquid-vapor phase transition.

Published: Laser Phys. Lett., vol. 14, p. 036001 (2017); DOI: 10.1088/1612-202X/aa539b

Interaction of laser pulses with solid and liquid targets, especially under conditions where phase transitions and/or surface tension are important, reveals a broad variety of physical phenomena, many of which find practical applications but pose serious challenges for theoretical modeling[1–4]. The focus of this work is on the dynamical behavior of spherical drops of liquid tin (Sn), irradiated by ultra-short (picosecond and sub-picosecond) laser pulses. This particular type of laser-induced target dynamics has an important area of application in laser-plasma sources of 13.5-nm extreme ultraviolet (EUV) emission for lithography[5,6], where fragmentation of Sn droplets with diameters of 20–50 μm by ps prepulses proved to be an effective way of target shaping for achieving high conversion efficiency into the 13.5-nm emission under the subsequent multi-nanosecond main pulse[7].

Previous studies in this direction have been mainly concentrated on either water[3,8] or tin drops[9], irradiated by multi-nanosecond laser pulses, where the target behavior differs dramatically from the impact of very short ps-scale pulses. The principal difference arises from the fact that, by a ps pulse, the pressure thrust lasts much shorter than the time of sound propagation ($\gtrsim 10$ ns) across the droplet. To the best of our knowledge, the present work is the first one where, using both the experimental data and simulation results, the main physical processes, leading to a unique morphology of spherical metallic drops shattered by ps laser pulses, are identified and analyzed. Though all the specific results, presented below, are for Sn droplets with a fixed diameter of $D_{dr} = 60$ μm, our main conclusions apply to the entire range of droplet sizes used in the EUV lithography.

The experiments have been performed on 60-μm droplets of liquid Sn-In eutectic alloy with the 48%–52% mass stoichiometry, generated by a commercial dispenser MJ-SF-01 by MicroFab Technologies. The melting temperature of this alloy, equal to 119°C, is almost two times lower than that of pure tin and indium. The vacuum experimental chamber had a residual pressure of $< 10^{-4}$ mbar and a working temperature of 140°C. A relatively low operating temperature allowed easier experimental conditions, keeping all the other physical properties of the alloy similar to the pure tin.

The main laser system consisted of a Ti:Sapphire generator (Spectra Physics Tsunami, $\lambda = 780$–820 nm), a regenerative amplifier (Spectra Physics SpitFire) and the pumping lasers (Spectra Physics Millennia eV Spectra Physics Empower). The regenerative amplifier allowed variation of the pulse duration τ from 50 fs to 5.3 ps; the latter was measured by means of the autocorrelation function with a PulseScout autocorrelometer. The experiments were performed at the maximum achievable pulse energy of 2.3 mJ. For visualization of the droplet dynamics we used the stroboscopic shadowgraphy by backlighting the object with 30-ns long pulses of a diode laser IL30C at $\lambda = 850$ nm. The shadow images were recorded by using a long distance microscope and a CCD camera. Further details on the experimental setup, synchronization and diagnostics can be found in Ref. 10.

A series of shadowgraphs in Fig. 1 shows how the shape of an initially spherical droplet evolves in time when hit by pulses with a fixed duration of $\tau = 5.3$ ps; the focal spot in all shots had a $1/e^2$ diameter of $D_{foc} = 72$ μm. The laser light propagates from left to right in the view plane at an angle of 17° with respect to the horizontal. The bright white spot, present on all shadowgraphs, corresponds to the hot plasma emission at, and immediately after, the laser pulse (captured by the camera due to its long exposure window). It may serve as a marker for the original position of the irradiated droplet hemisphere.

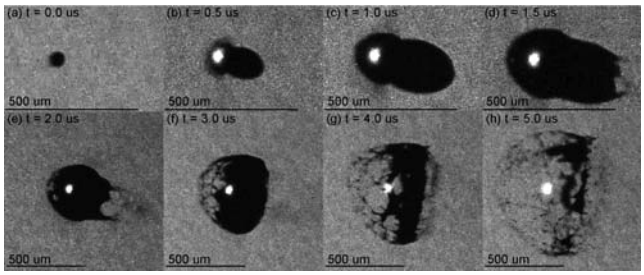

FIG. 1. Shadowgraphs of 60-μm droplets taken at different time delays t after the 5.3-ps laser pulse.

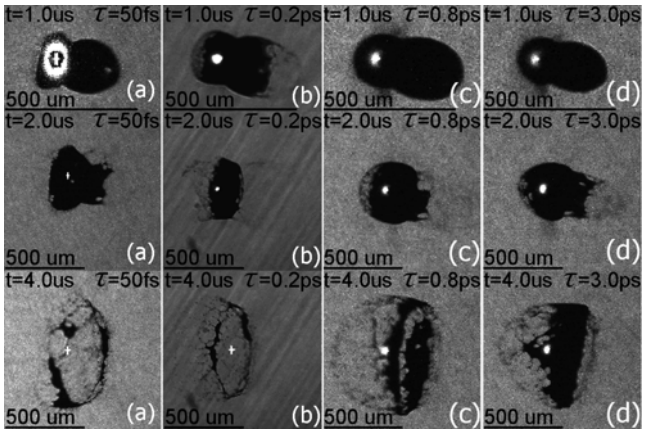

FIG. 2. Droplet shadowgraphs taken at $t = 1$ μs (upper row), $t = 2$ μs (middle row), and $t = 4$ μs (lower row) for different pulse durations τ: (a) 50 fs, (b) 0.2 ps, (c) 0.8 ps, (d) 3.0 ps.

Figure 1 clearly demonstrates that the hydrodynamic response of a metallic drop to an ultra-short laser impact strongly differs from that observed for ns pulses: instead of a thin flattened "pancake"[9], we observe an acorn-like shape, composed of two unequal conjunct spheroids, which continue to expand and gradually (starting from their polar caps) become translucent for the backlighting laser. At times $t \gtrsim 4$ μs the opaque target portion looks like a rugged ring-like shape. Figure 2, where the target evolution is shown for different pulse durations τ, varying over two orders of magnitude, confirms that the general features of the target behavior, revealed by our measurements, are rather insensitive to τ. Clearly, this behavior cannot be explained within the theoretical picture, developed earlier for the nanosecond pulses[8].

As a ps laser pulse hits a metallic droplet, its energy is deposited in a surface layer with a thickness well below 1 μm, and the resulting pressure pulse is generated on a timescale < 1 ns. The sonic time in our case is $D_{dr}/c_s = 24$ ns. Under such conditions, the key features of the hydrodynamic response could seemingly be understood in terms of the known self-similar solution of impulsive load[11] (Ch. XII, §13). However, we have two additional complications: (i) the pressure pulse is applied to a spherical rather than planar surface and has a spatially varying amplitude, and (ii) the equation of state (EOS) is not that of an ideal gas but must adequately account for the liquid-gas phase transition.

The results of two-dimensional (2D) simulations with the radiation-hydrodynamics code RALEF[12–14], including both mentioned factors, are shown in Fig. 3. The target shape in frame (c), calculated for $t = 1$ μs, quite closely resembles the corresponding experimental shadowgraphs (note that the plots in Fig. 3 are not shadowgraphs but 2D maps of pressure and density across the axial cut through a rotationally symmetric target). The latter implies that the theoretical model, implemented in the RALEF code, should already be sufficient to provide basic understanding of the physical processes, governing the observed dynamics of droplet deformation. At the same time, it is still not accurate enough to ensure satisfactory *quantitative* agreement between theory and observations.

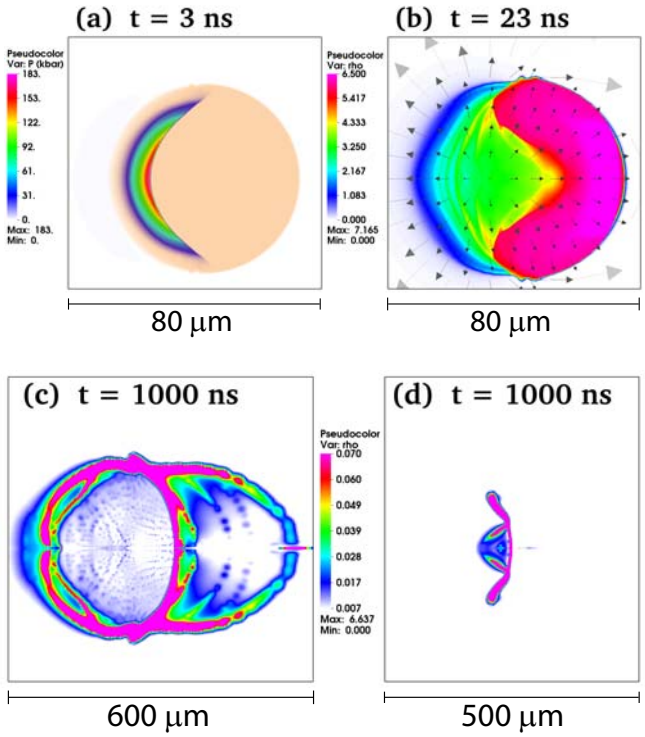

FIG. 3. Simulation results: (a) 2D pressure distribution behind the shock front at $t = 3$ ns; (b), (c) density distributions at $t = 23$ ns and 1 μs; arrows in (b) indicate the velocity field; (d) same as (c) but for a "harder" version of EOS with the tin critical pressure of 2.5 kbar[15]. Frames (a)-(c) represent square regions of size indicated by the ruler; the region in frame (d) has the same height as that in frame (c).

The simulated droplet had a diameter of 60 μm and was irradiated by a 1.5-ps long pulse with the same energy fluence of 113 J/cm^2 on the axis as in the experiment but with a larger spot of $D_{foc} = 130$ μm, for which the best agreement with the observed shape at $t = 1$ μs was found. Of the 2.6 mJ of the laser energy, hitting the droplet, 0.93 mJ was actually absorbed, of which about 0.09 mJ was reemitted as thermal x-rays and

$E_{tg} \approx 0.84$ mJ was left in the target material. However, more than 90% of E_{tg} resided in only 1–3% of the initial droplet mass, ablated from a thin surface layer; consequently, the latter acquired high velocity $\gtrsim 100$ km/s and by $t = 1$ μs left the computational domain (0.5 mm in radius). High expansion velocity of the thin heated layer implies a relatively short duration of the pressure pulse and applicability of the model of impulsive load. In result, the total energy of the expanding shell in Fig. 3c was split between $E_{sh,int} \approx 0.06$ mJ of its internal and $E_{sh,kin} \approx 0.01$ mJ of its kinetic energy.

Next we observe that, because $E_{sh,int}$ amounts to only a few percent of the 1.7 mJ needed for full vaporization of a 60-μm tin droplet, the major portion ($> 90\%$ of its initial mass) of the shattered droplet must be in the liquid state. Having evaluated the surface energy of a liquid shell by $t = 1$ μs as $E_{sh,\sigma} \approx 8\pi\sigma R_1^2 \approx 0.5$ μJ, we find that $E_{sh,\sigma} \ll E_{sh,kin}$; hence, the effect of surface tension $\sigma = 0.53$ N/m[16] on the overall shell dynamics can be safely neglected for times $t \leq 1$ μs. Note that this conclusion does not depend on the effective shell radius R_1 at the selected reference time $t = 1$ μs because, for a fixed droplet mass, both $E_{sh,kin}$ and $E_{sh,\sigma}$ scale as R_1^2 (note that $R_1 \approx 0.2$ mm in Fig. 3c, which is roughly twice the experimental value in Figs. 1 and 2).

The fact that the total energy $E_{sh,int} + E_{sh,kin}$, transferred to the main droplet mass and governing its subsequent dynamics, constitutes only a small fraction ($< 10\%$) of the net deposited energy E_{tg} provides an additional evidence for applicability of the impulsive load model[11], where the total energy of the expanding gas is infinite. At the same time, it suggests that adequate quantitative comparison between theory and experiments would require high-quality 2D hydrodynamic simulations combined with sufficiently accurate models for the laser absorption and for the EOS of tin in the region gas-liquid phase coexistence.

Thus, to gain insight into the fragmentation dynamics, we have to analyze the propagation of a shock wave, launched from the irradiated part of the droplet surface by a short and powerful pressure pulse. The 2D pressure distribution behind this shock at $t = 3$ ns is shown in Fig. 3a. Having started from a spherical surface, the shock initially has a distinct crescent shape. The shock pressure varies in time and space: it peaks on the laser-beam (polar) axis and drops to zero at the equator (somewhat steeper than $\cos\theta$ because of the increasing laser reflection at oblique incidence).

As predicted by the impulsive load solution[11], the shock pressure decreases as it propagates from left to right: starting from 1–2 Mbar at $t \lesssim 1$ ns, the pressure jump on the axis drops to 180 kbar by $t = 3$ ns (Fig. 3a), and then to $\simeq 20$ kbar at $t = 23$ ns (Fig. 3b), as the shock breaks out at the rear side. Simultaneously, because of a partial focusing of the crescent-shaped front, its attenuation is slowed down (or even reversed) near the droplet center, where a local entropy maximum is often observed.

On the pv diagram (p is the pressure, v the specific volume), shown in Fig. 4, all the fluid elements, set in motion by the shock, are represented by a limited segment of the Hugoniot curve, starting from the normal density. Having passed through the shock front, every fluid element is unloaded along its particular isentrope[11] (Ch. XI, §21). In the parameter range relevant to our experiments, all the unloading isentropes cross the binodal (boundary of the liquid-vapor phase coexistence region) from the liquid side (points B_1 and B_2). Adequate description of the unloading dynamics below the binodal requires, strictly speaking, a far more complex theoretical model than just hydrodynamics based on a certain EOS.

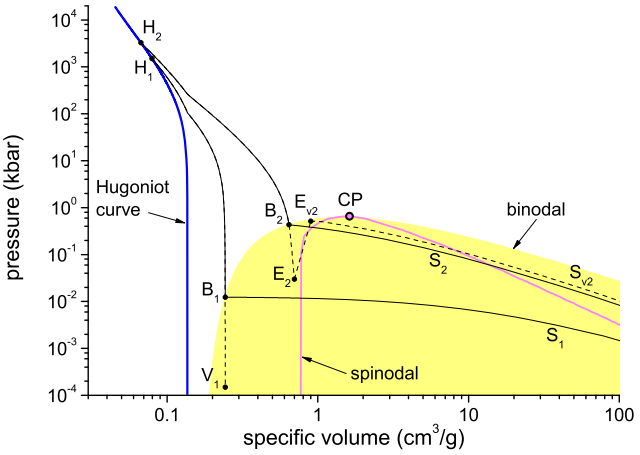

FIG. 4. Pressure-volume diagram of tin around the liquid-vapor phase coexistence region (shaded), constructed with the EOS model from Ref. 17. Thin solid curves $H_1B_1S_1$ and $H_2B_2S_2$ are equilibrium isentropes starting at different points on the Hugoniot curve. Metastable isentropes and a supposed explosive-boiling trajectory $E_2E_{v2}S_{v2}$ are shown with dashes. CP is the critical point from Ref. 18.

The RALEF simulations discussed here have been done within a simplified approach of pure hydrodynamics (without viscosity and surface tension but with heat conduction), based on the fully equilibrium EOS (EQ-EOS) obtained by means of Maxwell's construction in the two-phase region[17]. Here matter is treated as a homogeneous mixture of vapor and liquid (like fog), negative pressures do not exist, and the process of unloading under the binodal proceeds along equilibrium isentropes (B_1S_1 and B_2S_2 in Fig. 4); at the binodal the sound speed experiences a discontinuity. As was demonstrated in Ref. 1, this approach can already be sufficient to explain some remarkable effects of the ultra-short laser pulses.

In reality however, because of short (ns) timescales involved, the pure-liquid unloading isentrope must actually penetrate into the metastable (MS) region of superheated liquid until it either settles at a near zero pressure (segment B_1V_1)[11] (Ch. XI, §21) or, having approached the spinodal (the boundary of the region of absolute thermodynamic instability) and passed through the phase of explosive boiling (segment $B_2E_2E_{v2}$), continues along a

higher EQ isentrope $E_{v2}S_{v2}$[17]. If, in addition, the superheated liquid is stretched by a diverging velocity field, it may continue unloading into the negative-pressure domain (not shown in Fig. 4) and finally boil up (cavitate) near the $p < 0$ spinodal branch. Clearly, without proper modeling of the dynamics of metastable states and explosive boiling (like, for example, in an MS-EOS model proposed in Ref. 17), one can hardly expect good quantitative agreement between measurements and simulations.

Figure 3c tells us that an impulsive-load shock, applied from one side, transforms a liquid sphere into a shell, containing two cavities. The entire walnut-like shell is composed of two dome-like external walls and a third inner wall, separating the two cavities. The experimental shadowgraphs in Figs. 1 and 2 should be interpreted as the outer surfaces of the external dome walls. Note that in our simulations, because of the EQ-EOS approximation, the cavity walls are not pure-liquid films, separated from vapor by distinct surfaces, but just sharp density contrasts in the fog-like matter. As explained in Ref. 1, such density contrasts develop in rarefaction waves at the kink points (B_1 and B_2 in Fig. 4) of the equilibrium isentropes due to a jump-like decrease of the sound velocity.

Numerous RALEF simulations for varying target and laser parameters confirmed that the two-chamber target structure, shown in Fig. 3c, is a rather general result of an impulsive load, applied to a liquid sphere from one side. The primary cavity on the front (laser) side is a direct consequence of a diverging velocity field (see Fig. 3b), created by passage of the 2D shock front with pressure maximum on the rotation axis (Fig. 3a). Intuitively the least clear moment — namely, how a significant portion of the unloaded material behind a decaying shock acquires negative velocities — is explained in Ref. 11, Ch. XII, §15. Once the momentum of the diverging flow in a continuous liquid exceeds a certain limit, the liquid is ruptured (cavitates) and a central (primary) vapor chamber is formed.

The secondary (rear) cavity is a result of spall fracture and detachment of a thin liquid layer when the shock emerges from the rear surface — as it has, for example, been observed and explained for water droplets[4]. The equatorial bulb, observed in Fig. 3c where the three walls of the two cavities meet, represents a dense and massive ring, which is clearly visible on all experimental shadowgraphs at $t \gtrsim 3$ μs. This ring contains the coldest and densest portion of the initial droplet mass because the initial shock had the lowest amplitude there.

Qualitatively, the effects of cavitation and spallation are fairly reproduced by the 2D simulations with the EQ-EOS. However, it remains unclear how strongly would such quantitative characteristics, as the size and vapor density of the two cavities and their expansion velocities, change after a more adequate MS-EOS model is implemented. One thing is clear: while the EQ-EOS predicts that the wall density of the expanding shell drops in time (with the shell thickness remaining roughly constant), negative pressures in the MS-EOS model should, on the contrary, ensure a constant density of the liquid walls, forcing their thickness to diminish in time.

One of our key findings by theoretical modeling (more details are to be published elsewhere) is a high sensitivity of both the morphology and the rate of expansion of a shattered droplet to the details of EOS in the region of liquid-vapor phase transition, and, in particular, to the parameters of the critical point. As an illustration, Fig. 3d shows the simulation from Fig. 3c, repeated with the EQ-EOS parameters readjusted so as to shift the critical pressure of tin from $p_{CP} = 0.52$ kbar[18] (used as a regular option) to $p_{CP} = 2.5$ kbar as reported in Ref. 15. Evidently, the shape in Fig. 3d bears no resemblance to our experimental observations. Moreover, simulations do indicate that even much milder modifications of EOS incur significant and easily measurable changes in the morphology and/or expansion velocity of the shell-like structure, into which a spherical liquid-metal droplet is transformed by a short laser pulse.

The above analysis leads to a rather general conclusion that irradiation of spherical metallic droplets with ultrashort laser pulses provides a new sensitive instrument for probing the equation of state and the model for treatment of metastable states in liquid metals. One might even conjecture that such experiments open up a new area of applied research for thermophysical properties of metals in the hard-to-access region around the critical point and metastable liquid states. A combination of (i) a relatively simple theoretical picture of the phenomenon (a one-sided impulsive load upon a liquid sphere), (ii) easily measurable parameters of the expanding shell (its overall shape, relative sizes of the two domes, components of the expansion velocity, etc.) at times $t \gtrsim 1$ μs, and (iii) high sensitivity of the shell parameters to the details of EOS and the dynamics of metastable liquids gives a possibility to impose new tight constraints on the relevant theoretical models and, in particular, on the poorly known parameters of the critical points of metals. In the more narrow context of EUV lithography, adequate modeling of Sn droplet fragmentation by ps laser prepulses is of crucial importance for further optimization of the 13.5-nm emission under the subsequent main pulse.

This work was supported by the Ministry of Education and Science of the Russian Federation under the Agreement No. 14.579.21.0004, project RFMEFI57914X0004. The authors are grateful to N. Inogamov and V. V. Zhakhovskii for fruitful discussions.

[1] K. Sokolowski-Tinten, J. Bialkowski, A. Cavalleri, D. von der Linde, A. Oparin, J. Meyer-ter Vehn, and S. I. Anisimov, Phys. Rev. Lett. **81**, 224 (1998).

[2] N. A. Inogamov and V. V. Zhakhovskii, JETP Letters **100**, 4 (2014).

[3] A. L. Klein, W. Bouwhuis, C. W. Visser, H. Lhuissier, C. Sun, J. H. Snoeijer, E. Villermaux, D. Lohse, and H. Gelderblom, Phys. Rev. Applied **3**, 044018 (2015).

[4] C. A. Stan, P. R. Willmott, H. A. Stone, J. E. Koglin, M. Liang, A. L. Aquila, J. S. Robinson, K. L. Gumerlock, G. Blaj, R. G. Sierra, S. Boutet, S. A. H. Guillet, R. H. Curtis, S. L. Vetter, H. Loos, J. L. Turner, and F.-J. Decker, The Journal of Physical Chemistry Letters **7**, 2055 (2016).

[5]V. Bakshi, *EUV Sources for Lithography*, Press Monographs (SPIE Press, 2006).
[6]V. Y. Banine, K. N. Koshelev, and G. H. P. M. Swinkels, Journal of Physics D: Applied Physics **44**, 253001 (2011).
[7]H. Mizoguchi, H. Nakarai, T. Abe, K. M. Nowak, Y. Kawasuji, H. Tanaka, Y. Watanabe, T. Hori, T. Kodama, Y. Shiraishi, T. Yanagida, G. Soumagne, T. Yamada, T. Yamazaki, S. Okazaki, and T. Saitou, Proc. SPIE **9422**, 94220C (2015).
[8]H. Gelderblom, H. Lhuissier, A. L. Klein, W. Bouwhuis, D. Lohse, E. Villermaux, and J. H. Snoeijer, Journal of Fluid Mechanics **794**, 676 (2016).
[9]D. Kurilovich, A. L. Klein, F. Torretti, A. Lassise, R. Hoekstra, W. Ubachs, H. Gelderblom, and O. O. Versolato, Phys. Rev. Applied **6**, 014018 (2016).
[10]A. Y. Vinokhodov, K. N. Koshelev, V. N. Krivtsun, M. S. Krivokorytov, Y. V. Sidelnikov, S. V. Medvedev, V. O. Kompanets, A. A. Melnikov, and S. V. Chekalin, Quantum Electronics **46**, 23 (2016).
[11]Y. Zel'dovich and Y. Raizer, *Physics of Shock Waves and High-Temperature Hydrodynamic Phenomena*, Dover Books on Physics (Dover Publications, 2012).
[12]M. M. Basko, J. A. Maruhn, and A. Tauschwitz, Journal of Computational Physics **228**, 2175 (2009).
[13]M. M. Basko, J. A. Maruhn, and A. Tauschwitz, "Development of a 2D radiation-hydrodynamics code RALEF for laser plasma simulations," GSI Report 2010-1, PLASMA-PHYSICS-25 (GSI Helmholtzzentrum für Schwerionenforschung GmbH, 2010).
[14]M. M. Basko, Physics of Plasmas **23**, 083114 (2016).
[15]V. Y. Ternovoi, A. S. Filimonov, V. E. Fortov, I. V. Lomonosov, D. N. Nikolaev, and A. A. Pyalling, AIP Conference Proceedings **429**, 87 (1998).
[16]A. E. Vol and I. K. Kagan, *Handbook of Binary Metallic Systems: Structure and Properties, Volume 3; Systems of Gold, Indium, Iridium, Ytterbium and Yttrium* (National Bureau of Standards, Washington DC, 1985).
[17]S. Faik, M. M. Basko, A. Tauschwitz, I. Iosilevskiy, and J. A. Maruhn, High Energy Density Physics **8**, 349 (2012).
[18]D. S. Gates and G. Thodos, AIChE Journal **6**, 50 (1960).